Manuscript prepared for Geosci. Model Dev. Discuss.
with version 2014/09/16 7.15 Copernicus papers of the LaTeX class copernicus.cls.
Date: 26 June 2015

The Polar Vegetation Photosynthesis and Respiration Model (PolarVPRM): a parsimonious, satellite data-driven model of high-latitude CO_2 exchange

Kristina A. Luus[1] **and John C. Lin**[2,3]

[1]Biogeochemical Integration, Max Planck Institute for Biogeochemistry, Jena, Germany
[2]Atmospheric Sciences, University of Utah, Salt Lake City, USA
[3]Earth and Environmental Sciences, University of Waterloo, Waterloo, Canada

Correspondence to: Kristina A. Luus (kluus@bgc-jena.mpg.de)

Abstract

We introduce the Polar Vegetation Photosynthesis and Respiration Model (PolarVPRM), a remote-sensing based approach for generating accurate, high resolution ($\geq 1\,km^2$, three-hourly) estimates of net ecosystem CO_2 exchange (NEE). PolarVPRM simulates NEE using polar-specific vegetation classes, and by representing high-latitude influences on NEE, such as the influence of soil temperature on subnivean respiration. We present a description, validation, and error analysis (first-order Taylor expansion) of PolarVPRM, followed by an examination of per-pixel trends (2001–2012) in model output for the North American terrestrial region north of 55° N. PolarVPRM was validated against eddy covariance (EC) observations from nine North American sites, of which three were used in model calibration. Comparisons of EC NEE to NEE from three models indicated that PolarVPRM displayed similar or better statistical agreement with eddy covariance observations than existing models showed. Trend analysis (2001–2012) indicated that warming air temperatures and drought stress in forests increased growing season rates of respiration, and decreased rates of net carbon uptake by vegetation when air temperatures exceeded optimal temperatures for photosynthesis. Concurrent increases in growing season length at Arctic tundra sites allowed increases in photosynthetic uptake over time by tundra vegetation. PolarVPRM estimated that the North American high-latitude region changed from a carbon source (2001–2004) to sink (2005–2010) to source (2011–2012) in response to changing environmental conditions.

1 Introduction

Large uncertainties presently exist in process-based model estimates of high-latitude North American NEE (Fisher et al., 2014), and limit understanding and monitoring of recent changes in the polar carbon cycle. Simultaneously, recent successes in generating site-level, data-driven estimates of net ecosystem CO_2 exchange (NEE) at Arctic sites (e.g. Shaver et al., 2007, 2013; Stoy et al., 2009) with little inter-site variability in parameters (Lo-

ranty et al., 2011) have indicated the tremendous potential that exists for accurate estimates of regional-scale Arctic NEE to be modeled diagnostically from satellite observations.

In this article, we describe, validate, and examine output from the newly developed Polar Vegetation Photosynthesis and Respiration Model (PolarVPRM). PolarVPRM is an arctic-specific remote-sensing based model which estimates high-latitude net ecosystem CO_2 exchange (NEE) at a fine resolution (three-hourly, $\geq 1\,km^2$) using a diagnostic approach. PolarVPRM is presently in active use by the Arctic research community for a range of applications, including the examination and scaling up of circumpolar eddy covariance observations of NEE, and as a priori estimates of Alaskan NEE for Lagrangian modeling of aircraft CO_2 concentration observations (Miller and Dinardo, 2012).

1.1 PolarVPRM formulation

PolarVPRM presents a high-latitude formulation of VPRM (Mahadevan et al., 2008). Both PolarVPRM and VPRM were written in R (R Development Core Team, 2011), and provide straightforward yet effective calculations of terrestrial biospheric carbon exchange from remote-sensing observations. In both VPRM and PolarVPRM, NEE is calculated as the sum of respiration (R) and gross ecosystem exchange (GEE, the light-dependent portion of NEE), using the sign convention where CO_2 effux to the atmosphere via R is positive, and CO_2 uptake through photosynthesis (GEE) is negative:

$$\mathrm{NEE} = \mathrm{GEE} + \mathrm{R} \tag{1}$$

Relative to VPRM, PolarVPRM uses different inputs (described in Appendix A), vegetation classes (presented in Luus et al. (2013b)), and model structure (described in Luus et al. (2013a)), in order to ensure suitability for modeling high-latitude NEE. VPRM has previously been applied and validated across the USA and southern Canada (30–56° N) (Mahadevan et al., 2008; Lin et al., 2011), and PolarVPRM is now applied to generate estimates of NEE across high-latitude regions (e.g. north of 55 ° N).

1.1.1 Gross ecosystem exchange

Gross ecosystem exchange (GEE), or the photosynthetic uptake of C by vegetation, is calculated according to remote-sensing based estimates of incoming shortwave radiation (SW, expressed as photosynthetically active radiation (PAR, where PAR $= 1.98 \times$ SW; Lin et al., 2011), air temperature (T_{air}), land surface water index (LSWI) from Moderate Resolution Imaging Spectroradiometer (MODIS) surface reflectance, and estimates of the fraction of PAR absorbed by photosynthetically active vegetation ($FAPAR_{PAV}$), as estimated from the MODIS Enhanced Vegetation Index (EVI).

In Arctic tundra regions, GEE is therefore implicitly limited during the snow season, when EVI is decreased, suggesting that negligible amounts of photosynthetically active vegetation persist above the snow surface. Similarly, GEE can be limited when air temperatures are suboptimal, or when vegetation is at an underdeveloped phenological stage. These limitations are implemented through use of dimensionless scaling variables T_{scale} and P_{scale}, respectively.

$$P_{\text{scale}} = \frac{1 + \text{LSWI}}{2} \tag{2}$$

$$W_{\text{scale}} = \frac{1 + \text{LSWI}}{1 + \text{LSWI}_{\text{max}}} \tag{3}$$

$$T_{\text{scale}} = \frac{(T_{\text{air}} - T_{\text{min}})(T_{\text{air}} - T_{\text{max}})}{(T_{\text{air}} - T_{\text{min}})(T_{\text{air}} - T_{\text{max}}) - (T_{\text{air}} - T_{\text{opt}})^2} \tag{4}$$

$$\text{GEE} = -1 \cdot (\lambda \cdot T_{\text{scale}} \cdot W_{\text{scale}} \cdot P_{\text{scale}}) \cdot \text{FAPAR}_{\text{PAV}} \cdot \frac{1}{1 + \frac{\text{PAR}}{\text{PAR}_0}} \cdot \text{PAR} \tag{5}$$

λ refers theoretically to the maximum light use efficiency, or quantum yield, at low light levels, but functions in practice as a combined LUE and scaling parameter. PAR_0 is the half-saturation value of PAR (Mahadevan et al., 2008; Lin et al., 2011). As in Mahadevan et al. (2008), T_{max}=40° C and T_{min}=0° C for all vegetation classes, and T_{opt}=20° C for non-arctic

vegetation classes. For barren/wetland regions (which include the Canadian High Arctic), a T_{opt}=10° C, whereas T_{opt}=15° C over shrub tundra and graminoid tundra, as approximated from literature (e.g. Tieszen (1973); Chapin III (1983)). Plots of air temperature and growing season NEE at calibration sites were checked to ensure that these values appeared reasonable, but no optimization took place, to avoid correlation and instability of parameters (Mahadevan et al., 2008).

$LSWI_{max}$ refers to the maximum annual pixel-specific LSWI. LSWI is implemented as a limitation on GEE (W_{scale}) for forested regions north of 55° N, just as in VPRM. However, water availability does not play a clear role in determining Arctic plant productivity (Oberbauer and Miller, 1979; Chapin III and Shaver, 1985; Shaver et al., 1986; Johnson and Caldwell, 1975) due to the unique prevailing environmental conditions. In wetland regions, water can both stimulate and limit plant productivity. Snowmelt provides a large portion of annual precipitation to Arctic regions, and the high humidity of growing season conditions limits water loss. Water tables are above or at the ground surface in moist/wet tundra ecosystems, and beneath or at the rooting level in shrub/dry tundra (Chapin III et al., 2000). Permafrost both limits percolation past the rooting depth, and provides an added input of water to plant roots throughout the growing season (Oberbauer and Dawson, 1992). In low Arctic regions, water availability is therefore not linearly associated with plant productivity (Oberbauer and Miller, 1979; Miller, 2006; Chapin III and Shaver, 1985).

In polar desert regions, surface drying can occur despite ongoing saturation of subsurface soils, and surface drying therefore has little biological influence on plant productivity (Gold and Bliss, 1995). Water does have an indirect influence in determining Arctic vegetation species distributions due to its role in germination (Bliss, 1958); however, in PolarVPRM, Arctic tundra vegetation remains within the same allocated vegetation class (i.e. graminoid tundra, shrub tundra, or barren/wetland) throughout model runs ($<$ 20 years). W_{scale} is therefore always set to 1 for regions with tundra vegetation, and is calculated according to LSWI in forested areas of NAHL.

1.1.2 Respiration

VPRM and PolarVPRM simulate respiration (R) as a function of temperature, where R encompasses autotrophic and heterotrophic respiration. During the growing season, a larger portion of R arises from aboveground autotrophic respiration, and a smaller portion of R arises from soil respiration. Growing season R is therefore more heavily influenced by aboveground than belowground temperatures, and so growing season R is simulated in VPRM and PolarVPRM as a function of air temperature. In VPRM, R is estimated year-round as a piecewise linear function of air temperature, meaning that R is set to a low constant value throughout the portion of the year when air temperatures are low.

In PolarVPRM, snow season R is calculated according to soil temperature, rather than air temperature, because rates of subnivean respiration are driven primarily by soil temperature rather than air temperature (Grogan and Jonasson, 2006; Sullivan et al., 2008; Morgner et al., 2010). Arctic field studies have shown that a large portion of annual carbon efflux can occur during the snow season (Aurela et al., 2004; Sullivan et al., 2008; Elberling and Brandt, 2003), and that the low thermal conductivity of an overlying snowpack (e.g. $0.06\,\mathrm{W\,(m^{\circ}C)^{-1}}$ Sturm, 1992) substantially decouples Arctic soil and air temperatures (e.g. by 10–40 °C (Zimov et al., 1993), or by 15–20 °C Olsson et al., 2003). Calculating snow season R according to soil temperature, rather than setting R to a low constant value like in VPRM, is therefore likely to better capture inter-annual and seasonal variability in snow season NEE, and reduce uncertainty in annual Arctic C budgets (Luus et al., 2013c).

Accuracy in estimates of Arctic R throughout the snow and growing seasons is maximized by first demarcating the snow and growing seasons according to Moderate Resolution Imaging Spectroradiometer (MODIS) observations of fractional snow cover area (SCA) (Appendix A), since filtered MODIS estimates of SCA agree well with in situ observations of SCA (Luus et al., 2013a).

Snow season ($\mathrm{SCA} \geq 50\,\%$) respiration is then calculated as a linear function of soil temperature, and growing season respiration ($\mathrm{SCA} < 50\,\%$) is calculated as a piecewise linear

function of air temperature:

$$\mathrm{R} = \begin{cases} \alpha \cdot T_{\mathrm{air}} + \beta : & \mathrm{SCA} < 50\,\% \\ \alpha_{\mathrm{s}} \cdot T_{\mathrm{soil}} + \beta_{\mathrm{s}} : & \mathrm{SCA} \geq 50\,\% \end{cases} \tag{6}$$

Calculating subnivean respiration from soil temperature and growing season respiration from air temperature decreased model errors at two high-latitude sites (Daring Lake & Ivotuk), relative to other model formulations using only either soil or air temperatures alone, including the original VPRM (Luus et al., 2013a). At all three Arctic calibration sites, R^2 values were larger when respiration was regressed linearly from air temperature, than when exponential or Q10 functions were used to describe these associations, likely because Arctic rates of respiration are low, and therefore only the low part of the exponential curve is captured. Furthermore, statistical tests with data from Ivotuk (2004–7) using Akaike's Information Criterion found lower AIC scores when respiration was estimated from air and soil temperatures, than when respiration was estimated from air temperature alone. These AIC scores indicate that model quality is improved by the inclusion of soil temperature, despite the concurrent increase in model complexity.

1.1.3 PolarVPRM parameterization by vegetation class

High-latitude vegetation is heterogeneous, resulting in large variability in NEE and its drivers by vegetation type (Humphreys and Lafleur, 2011; Elberling, 2007). PolarVPRM therefore separates high-latitude vegetation into seven classes using a combination of the Synergistic Land Cover Product (SYNMAP) (Jung et al., 2006) and the Circumpolar Arctic Vegetation Map (CAVM) (Walker et al., 2005) (Table 1). CAVM is available only above the northernmost treeline, whereas SYNMAP is available globally. CAVM estimates are therefore used wherever available, and SYNMAP estimates are used to classify vegetation south of the CAVM treeline. The combined CAVM-SYNMAP vegetation classification is available at a $1\,\mathrm{km} \times 1\,\mathrm{km}$ resolution, and can be upscaled when coarser resolution ($\geq 1\,\mathrm{km}^2$) PolarVPRM outputs are desired.

Levene's Test was previously applied to determine whether the CAVM-SYNMAP classes in Table 1 delineate pan-Arctic groupings with heterogeneous distributions of passive microwave derived estimates of Arctic NEE drivers. These included cold season snow water equivalent, and growing season soil moisture, air temperature, and vegetation opacity. Findings indicated that for all passive microwave estimates examined, the CAVM-SYNMAP classes divided the pan-Arctic region into distributions with heterogeneous variances (p-value$<10^{-5}$), and which all displayed homoscedasticity over time ($0.5 \geq p$-value $\geq$0.99) (Luus et al., 2013b). The distinct distributions of the vegetation classes used, and their stability of variances over time, both indicate suitability for modeling purposes.

The North American high-latitude (NAHL) spatial resolution selected for this project is $1/6^\circ \times 1/4^\circ$ (latitude $\times$ longitude), and so vegetation classes are regridded accordingly. Each pixel is characterized by its fractional cover by one or more vegetation classes, and by its fractional water/glacier cover. NEE is calculated separately for each vegetation class, and total NEE for each pixel is calculated by multiplying the NEE for each vegetation class by its fractional cover.

Six separate parameters are used in the calculation of NEE across each vegetation class. All parameters are set empirically from associations found between meteorological and eddy covariance (EC) tower observations at one calibration site per vegetation class. Two parameters are used to calculate GEE (Eq. 5), and four parameters are used to calculate respiration (Eq. 6):

- PAR_0 describes the sensitivity of photosynthetic uptake to the quantity of incoming shortwave radiation
- λ represents light use efficiency of vegetation, and also acts as a scaling parameter
- α and β regression coefficients describe the linear association between growing season respiration and air temperature
- α_s and β_s regression coefficients describe the linear association between soil temperature and snow season respiration

1.1.4 PolarVPRM inputs

PolarVPRM remote sensing observations of the land surface were acquired from the Moderate-resolution Imaging Spectroradiometer (MODIS), and meteorological observations were acquired from the North American Regional Reanalysis (NARR), at the native spatial and temporal resolutions summarized in Table 2. All inputs were then regridded to the PolarVPRM spatial domain (NAHL, $1/6^\circ \times 1/4^\circ$ latitude $\times$ longitude) using bilinear interpolation in R. MODIS was linearly interpolated to three-hourly timesteps. PolarVPRM was run at NARR's native temporal resolution (three-hourly), although it could easily be run at a finer spatiotemporal resolution with higher resolution inputs. For a complete discussion of the changes made to model inputs, and reasons why specific meteorological products were selected, please refer to Appendix A.

1.2 Calibration and validation sites

PolarVPRM was calibrated and validated using standard meteorological observations and open-path eddy covariance measurements of NEE collected at HL North American sites (Table 3; Fig. 1). All parameters except λ were set according to half-hourly EC and meteorological observations, and λ was set using observations averaged to three-hourly timescales to match the temporal resolution of PolarVPRM.

Atqasuk (AT) and Barrow (Ba) are both located on the North Slope of Alaska, and were designated as paired calibration/validation sites representing barren/wetland vegetation in PolarVPRM. Field observations at the main Barrow EC site have indicated full flooding following snowmelt, with vegetation that consists mainly of wet sedges, moss, lichens and grasses (Oechel et al., 1995; Harazono et al., 2003). The Atqasuk EC site is located $\approx$ 100 km south of Barrow, and is both warmer and drier than the Barrow site. The predominant vegetation at Atqasuk is moist-wet sedge, underlain by wet, acidic soils (Kwon et al., 2006). Due to the similarity of these sites, they have previously acted as paired sites in studies of the Arctic carbon cycle (Hollister et al., 2005; Huemmrich et al., 2010).

Imnavait (Im) and Ivotuk (IV) are moist tussock tundra sites which were paired for calibration/validation, and represent the graminoid tundra vegetation class in PolarVPRM. Imnavait is located in the foothills north of the Brooks Range, in a region largely dominated my moist acidic tussock tundra (Euskirchen et al., 2012). Ivotuk is a moist acidic tussock tundra site located $\approx 200\,\mathrm{km}$ south of Atqasuk (Thompson et al., 2006; Laskowski, 2010), and Imnavait is located $\approx 200\,\mathrm{km}$ east of Ivotuk. The similarities in predominant vegetation, and geographical proximity, allowed these two sites to be paired.

The main Daring Lake (DL) EC site is located in a region of mixed tundra, in Canada's Northwest Territories (Lafleur and Humphreys, 2008; Humphreys and Lafleur, 2011). Observations from this site were used to calibrate the shrub tundra vegetation class. Since no other year-round EC observations were available at NAHL sites designated as shrub tundra from 2001–2012, validation for this class consisted of characterizing model performance over years which were not used for validation, and by describing the performance of this parameterization in describing NEE at Ivotuk (IV).

Meteorological and EC observations were collected during a portion of the 2008 growing season by (Lafleur et al., 2012) at Canadian high Arctic sites: Lake Hazen (lh), Cape Bounty (cb), Pond Inlet (pi), Iqaluit (iq). Observations from these sites were used as model validation for the graminoid and shrub tundra classes.

2 Methodology

Briefly, PolarVPRM estimates of three-hourly NEE were validated against observations from nine North American sites, and a detailed error attribution was then conducted using observations from two validation EC tower sites. Output from PolarVPRM and two existing models (CarbonTracker and FLUXNET Multi-Tree Ensemble) were then compared relative to EC observations. Changes over time (2001–2012) in PolarVPRM estimates of carbon cycling were then examined at various spatial scales across the entire high-latitude (north of 55° N) North American terrestrial region, hereafter referred to as NAHL, for the 2001–2012 time period.

2.1 Calibration

Sites with year-round eddy covariance observations (Fig. 1) were first described using the combined CAVM and SYNMAP classification (Table 1), and then paired. The CAVM and SYNMAP combined classification was specifically designed to allow for ecological differences resulting in varying flux drivers to be well represented, while ensuring that no category would be created that could not be parameterized using the existing eddy covariance infrastructure. If more year-round flux towers existed, then further distinctions could have been made between vegetation classes (e.g. barren/wetland).

Atqasuk, Ivotuk and Daring Lake were then selected as the calibration sites because they alone shared year-round observations during a single common year (2005). Parameter values for PolarVPRM's three Arctic tundra vegetation classes were then set using half-hourly observations from EC and meteorological towers collected at Daring Lake, (Lafleur and Humphreys, 2008; Humphreys and Lafleur, 2011), Ivotuk (Laskowski, 2010), and Atqasuk (Laskowski, 2010) (Fig. 1). In all cases, observations of NEE were filtered only to remove observations collected during instrument malfunction or when frictional velocity was low ($u^* < 0.2$) (Goulden et al., 1996). No gap filling was carried out for any of the EC measurements, as gap filling requires the application of another model and therefore does not represent a direct measurement of CO_2 flux (Barr et al., 2004).

Respiration parameters were set using simple linear regressions of air temperature and nighttime NEE (α and β), or subnivean soil temperature and snow season NEE (α_s and β_s). PAR_0 was set according to a non-linear least squares fit of PAR and GEE, using the `nls` function in R (R Development Core Team, 2011). The light use efficiency and scaling parameter (λ) was set to be equal to the slope from a linear regression of PolarVPRM GEE vs daytime growing season NEE, and was jointly optimized with PAR_0.

These parameters remained unchanged for all simulations, and were applied to generate regional estimates, as well as estimates at calibration and validation sites. Parameters for vegetation classes south of the treeline were set according to the VPRM parameterizations found in Mahadevan et al. (2008). Please refer to Mahadevan et al. (2008) for a detailed

description of the eddy covariance study sites used for calibration/validation purposes, the calibration approach used, and results indicating good predictions of monthly NEE over forested eddy covariance calibration sites, and their respective cross-validation sites.

Following model calibration at high-latitude sites, PolarVPRM estimates of GEE, respiration and NEE were generated for the entire North American region north of 55° N for years 2001–2012 at a three-hourly timestep and a spatial resolution of $1/6^\circ \times 1/4^\circ$ (latitude $\times$ longitude). The output from these simulations was used to conduct error analysis, validation, model intercomparisons, and trend analysis.

2.2 Validation

Validation consisted of examining model performance both over paired calibration/validation sites (AT, Ba, IV, Im), as well as growing season validation sites (lh, cb, pi, iq, ch). These sites capture a wide variety of vegetation types and regions of the North American arctic, especially in light of the small total number of sites in this region with continuous year-round observations during the MODIS era (2000–).

Model evaluation consisted of examining the Mean Bias Error (MBE) and Root Mean Squared Error (RMSE) between PolarVPRM estimates of mean three-hourly, daily and monthly average NEE (pred_i), and EC measurements of NEE (obs_i) at matching temporal resolutions:

$$\text{MBE} = n^{-1} \sum_{i=1}^{n} \text{pred}_i - \text{obs}_i \tag{7}$$

$$\text{RMSE} = \left[n^{-1} \sum_{i=1}^{n} |\text{pred}_i - \text{obs}_i|^2 \right]^{1/2} \tag{8}$$

Validation was conducted against 2005 EC observations at the three calibration sites (DL, AT, IV), and against observations from 2008 and 2001 at Im and Ba, respectively. 2008 and 2001 were selected as these were the closest years to 2005 for which year-round observations existed. After error metrics were calculated, plots comparing modeled and

observed values of NEE were generated to assist in identifying biases in modeled NEE. Validation was also conducted using observations of NEE collected in July 2008 by (Lafleur et al., 2012) from four Canadian Arctic sites (cb, iq, lh and pi).

Mean daily comparisons of NEE were used because of the large number of gaps found in eddy covariance observations, and the decision to not apply any gap-filling approaches to the flux data, as this would then constitute an inter-model comparison rather than a comparison of model estimates against eddy covariance observations. To ensure that these daily flux estimates would not be biased relative to model estimates in situations where more gaps in flux observations occurred at night rather than during the day, model estimates corresponding to time periods with missing observations were not included when calculating mean daily NEE. Validation therefore described the fit between model output, and in situ observations of NEE.

2.3 Error analysis

Due to the simple mathematical formulation of VPRM and PolarVPRM, uncertainties in estimates of NEE can be easily partitioned into systematic versus random errors (Lin et al., 2011). Systematic errors or biases cause model output to be offset in a specific direction, whereas random errors introduce additional and erroneous fluctuations in value. In order to better understand the deviation between PolarVPRM estimates of NEE and EC measurements of NEE, a comprehensive error analysis was completed according to the framework developed by (Lin et al., 2011), which is based on a first-order Taylor expansion.

Within this framework, errors are quantified by examining model estimates against eddy covariance observations at two year-round validation sites, Imnavait (Im) and Barrow (Ba), which had not been used in model calibration. Errors are then classified as either systematic or random. Errors are then attributed to input variables and parameters, and their total contributions to uncertainty in estimates of NEE are examined. Biases occurring due to input variables are addressed by comparing inputted shortwave radiation, soil temperature and air temperature, to NARR-derived estimates of these variables, and examining the portion of error in NEE arising from these discrepancies. Typically, model runs rely on

using parameters fitted at the calibration sites (Ivotuk and Atqasuk, respectively). Biases occurring due to mis-parameterization were assessed by first fitting all parameters using EC and meteorological observations from the validation sites (Im & Ba), then comparing model NEE generated using calibration-site parameters (IV & AT), to model NEE generated using site-specific parameters (from Im & Ba, respectively). Plotting the contribution of each component to model error then allows their relative contributions to be assessed.

2.4 Model inter-comparison

PolarVPRM estimates of NEE were compared against estimates of NEE by existing models with different formulations. All models were compared against EC NEE, which was upsampled from a half-hourly temporal resolution to three-hourly, daily and monthly time periods. Daily and three-hourly averages were created using only model estimates for which concurrent EC NEE observations had been collected, in order to complete analysis without gap-filled EC NEE data.

The models selected for inter-comparison were CarbonTracker CT2011_oi and FLUXNET Model-Tree Ensemble (MTE). CarbonTracker (Peters et al., 2007) and FLUXNET MTE (Jung et al., 2009) were selected on the basis that both provide estimates of NEE over northern regions, and both use approaches which are different from one another and from PolarVPRM.

CarbonTracker derives estimates of CO_2 surface fluxes by analyzing atmospheric CO_2 observations using a transport model (Transport Model 5, TM5) (Krol et al., 2005) in combination with a land surface biospheric flux model (Carnegie-Ames-Stanford Approach, CASA) (Potter et al., 1993) and fossil fuel inventories. One identified source of uncertainty in CarbonTracker estimates is from measurement errors or biases in CO_2 dry mole fractions (Masarie et al., 2011). FLUXNET MTE generates regional estimates of NEE by first training an ensemble of model trees using EC measurements from FLUXNET sites and inputs from the Lund–Potsdam–Jena managed Land (LPJmL) model (Bondeau et al., 2007), and then upscaling these measurements accordingly. Uncertainty in FLUXNET MTE estimates

of NEE has previously been through assessment of GPP simulated by LPJmL (Jung et al., 2009).

Estimates of NEE by PolarVPRM, CarbonTracker and FLUXNET MTE were spatially averaged for the entire terrestrial region north of 55° N at a monthly resolution for each year (2001–2012). Visual examination of Fig. 3, showing monthly average NEE for each model, provided insights into differences in high-latitude carbon cycling estimated by these models. Further analysis then consisted of creating similar plots examining PolarVPRM and CarbonTracker model output at distinct time slices (Fig. 4), as both of these models are available at a three hourly resolution. In order to create these plots, a distinct time of day was selected for each plot, and model estimates were then spatially averaged over the North American high-latitude domain, and averaged for each month of each year. Analysis of these plots highlighted differences in the representation of diurnal patterns in high-latitude NEE.

PolarVPRM, CarbonTracker and FLUXNET MTE estimates of three-hourly and mean monthly NEE were then compared against three-hourly and monthly observations of NEE available at the PolarVPRM calibration and validation sites for which annual observations were available: Atqasuk, Barrow, Daring Lake, Imnavait and Ivotuk.

2.5 Trends (2001–2012)

Changes over time in the high-latitude carbon cycle were first examined by plotting total CO_2 exchange across the North American high-latitude (NAHL) model domain to determine the relative contributions of respiration and photosynthesis (Fig. 5). Although recognized model uncertainties and the impossibility of thoroughly evaluating PolarVPRM performance across the heterogeneous model domain with current infrastructure limit confidence in estimates of the total carbon balance, examination of relative changes in CO_2 exchange over time and its drivers provide insights into responses of the high-latitude carbon cycle to recent environmental changes.

Trends over time were examined first for each year and each vegetation class, and then pixel-by-pixel across the entire model domain (Figs. 6–10). The non-parametric slope estimator (Sen's slope) (Sen, 1968) was applied to each pixel to determine the trend during the

years 2001–2012 of NEE, GEE and respiration. All calculations of Sen's slope values and their significance were conducted in R using the `rkt` package (Marchetto, 2012).

To further understand the specific influences driving these shifts, changes over time in carbon cycle variables and driver data were separately analyzed over the snow season (SS) and growing season (GS). These time periods were differentiated using MODIS MOD10A2 snow cover area (SCA), as a previous study indicated that remote-sensing estimates of 50 % SCA can accurately capture the timing of seasonal transitions in the low Arctic (Luus et al., 2013a). Changes over time in model inputs/outputs describing land surface characteristics are therefore described annually, as well as over the snow season (when SCA $\geq$ 50 %). Estimates of model variables over the growing season are limited to the portion of the year for which the land surface is snow free and for which vegetation is photosynthetically active (SCA $<$ 50 % AND GEE $<$ 0). This was done so that different insights could be gained into annual GEE and respiration, vs. GEE and respiration during the active growing season. The Sen's slope estimates of median changes in carbon cycle and land surface variables over time (2001–2012) were then reported for each pixel in the model domain corresponding to significant (p value $<$ 0.05) change.

3 Results and discussion

3.1 Validation

PolarVPRM three-hourly estimates of NEE showed excellent agreement with three-hourly averaged NEE measured at four Canadian Arctic sites during the 2008 growing season (Lafleur et al., 2012). The mean RMSE across all sites was 0.79 µmol CO_2 m^{-2} s^{-1}, and was largest at Iqaluit (1.01 µmol CO_2 m^{-2} s^{-1}) and smallest at Cape Bounty (0.66 µmol CO_2 m^{-2} s^{-1}) (Table 4). Although these errors are not negligible, the values are quite low considering the large distances between calibration sites and growing season validation sites (Fig. 1), as well as the large inter-site environmental differences (Lafleur et al., 2012).

Biases in NEE at these sites arose mainly due to biases in NARR shortwave radiation and air temperature. At Lake Hazen, NARR air temperatures were 10 °C colder on average than observed air temperatures, leading both photosynthesis and respiration to be underestimated. Furthermore, EVI remained low at Lake Hazen (< 0.1) and Iqaluit (< 0.2) throughout July 2008. Photosynthesis at these sites, and total net C uptake in July 2008, was therefore underestimated at these sites (lh MBE $= 0.39$, iq MBE $= 0.15$). At Cape Bounty and Pond Inlet, NARR shortwave radiation was substantially larger than observed, such that cb measured PAR $\approx 1.3 \times$ cb NARR SW radiation, and iq measured PAR $\approx 1.6 \times$ iq NARR SW radiation. These biases in shortwave radiation cause overall rates of photosynthesis and net C uptake at these sites to be overestimated (cb MBE=-0.33, pi MBE=-0.44). Despite the small biases introduced from meteorological inputs, PolarVPRM growing season observations agree relatively well with observations from remote Canadian Arctic sites (mean RMSE=0.79).

3.2 Error analysis

Comparisons of PolarVPRM NEE against observations of NEE at year-round calibration and validation sites indicated that PolarVPRM tended to slightly underestimate net C uptake by vegetation at validation sites (Barrow and Imnavait). The underlying reasons for the bias in net C uptake at year-round validation were addressed through a comprehensive error analysis.

The cumulative monthly bias in PolarVPRM, expressed as the difference between PolarVPRM modeled NEE and observed NEE ($\mathtt{model-observed}$), is indicated for two validation sites, Barrow and Imnavait in Fig. 2. In this figure, a positive bias in NEE indicates that either respiration was overestimated, or that photosynthetic uptake by vegetation was underestimated. Therefore, according to the sign convention used for NEE, a positive bias in respiration indicate that PolarVPRM overestimated respiration, whereas a positive bias in GEE indicates that PolarVPRM underestimated photosynthetic uptake by vegetation.

The main sources of error in PolarVPRM arose from biases in how the associations between PAR and GEE, and between λ and GEE, were parameterized (Fig. 2). NARR air

temperature and soil temperature agree closely with observed soil and air temperatures, meaning there is very little bias in estimates of respiration. Small errors in NARR shortwave radiation relative to observations caused small ($< 1\,\mathrm{g\ C\,m^{-2}}$) cumulative biases in net C exchange at these validation sites.

At Barrow (Ba) and Imnavait (Im), the amount of carbon taken up through photosynthesis is underestimated due to biases in λ, the light use efficiency and scaling parameter (Eq. 5). At the calibration sites, Atqasuk (AT) and Ivotuk (IV), λ values of 0.15 and 0.04 were identified as being optimal values for barren/wetland regions and graminoid tundra sites, respectively. When optimal λ were instead calculated using EC NEE from validation sites (Ba and Im), these yielded values of 0.29 and 0.34, respectively. These differences in optimal parameter values are caused by vegetation at the calibration sites (AT and IV) having a diminished photosynthetic response to light, especially at low light values, relative to plants at validation sites (Ba and Im). The use of sub-optimal λ values (calculated from AT and IV) in estimates of NEE at validation sites (Ba and Im) caused PolarVPRM to underestimate GEE, resulting in a bias in model estimates of NEE.

A recent study by (Dietze et al., 2014) likewise identified misparameterization of light-use efficiency at low light levels to play a central role in biospheric model uncertainties across HL regions of North America. The study indicated that a likely source for misparameterization is due to greater variance in this parameter across high-latitude sites, even when these contain similar biota. Although PolarVPRM calibration and validation sites were paired on the basis of having similar physical and biological characteristics, important differences appear to exist in the drivers of NEE at these sites, which are not captured by PolarVPRM. In order to identify whether the calibration or validation LUE values are more representative across HL tundra sites, a larger network of HL EC towers and measurements of light-response curves using leaf-level observations of gas exchange (Bernacchi et al., 2013) would be required.

A portion of the error observed at Barrow and Imnavait arises due to biases which are not considered in the error analysis framework. The gap between the sum of all biases and the total error is evident at both Barrow and Imnavait (Fig. 2). The error analysis approach

used is based on a first-order Taylor expansion, and therefore does not consider second order effects (Lin et al., 2011). As PolarVPRM has a simple model structure, it is likely that a portion of the bias arises due to incomplete characterization of the processes which drive carbon cycling. Future work will consist of further improving the accuracy of PolarVPRM estimates. Spatial heterogeneity in rates of respiration and CO_2 release from permafrost could be better represented by including satellite-derived maps of permafrost information (e.g. Heim et al., 2011). Estimates of PolarVPRM GEE could also be improved in the future once capabilities exist to accurately estimate vegetation fluorescence or photosynthetic stress from the Photochemical Reflectance Index (Grace et al., 2007; Hilker et al., 2008) across vast Arctic regions. Overall, although mis-parametrization of λ at the validation sites accounts for the most significant portion of error at Barrow and Imnavait, a hidden bias in NEE exists that compensates for the bias in λ, resulting in smaller net biases in NEE than would be expected through error decomposition.

3.3 Model inter-comparison

PolarVPRM shows closer agreement with EC NEE from five Arctic sites, than FLUXNET MTE shows against the same five sites (Table 5), indicating that PolarVPRM provides an improved data-driven approach for estimating regional-scale Arctic NEE. When three-hourly, daily and monthly averages of PolarVPRM and CarbonTracker were compared to EC NEE from five sites at same timescales, PolarVPRM had the lowest mean RMSEs for all timescales, and lower MBEs at monthly timescales, but larger MBEs at daily and three-hourly timescales. PolarVPRM therefore provides estimates of NEE which show similar or improved realism relative to EC NEE, using a simpler framework than CarbonTracker.

Comparisons of mean monthly NEE by PolarVPRM, Carbon-Tracker and FLUXNET Model-Tree Ensemble over NAHL indicated that both CarbonTracker and PolarVPRM estimated very low rates of mid-winter respiration, whereas the FLUXNET Model-Tree Ensemble (MTE) showed greater rates of mid-winter respiration (Fig. 3). FLUXNET MTE also estimates greater photosynthetic uptake of carbon by vegetation than the other two models.

The seasonal cycle and inter-annual variability displayed by PolarVPRM and CarbonTracker are very similar (Fig. 3).

Relative to CarbonTracker, PolarVPRM estimates less carbon to be taken up by vegetation photosynthetically at midday (18:00 UST), and estimates less respiration to occur in the middle of the night during the growing season (06:00 UST) (Fig. 4). However, when three-hourly estimates of NEE by PolarVPRM and CarbonTracker are compared against three-hourly EC measurements of NEE, PolarVPRM is found to have lower RMSE values than CarbonTracker (Table 5). CarbonTracker has a lower summed MBE than PolarVPRM because PolarVPRM more substantially underestimates peak growing season GEE at Daring Lake than CarbonTracker does, and this bias is disproportionately large as EC NEE is only available at Daring Lake during the growing season (unlike other sites). If three-hourly and daily MBEs were instead summed over remaining sites, PolarVPRM would have lower MBEs than CarbonTracker.

PolarVPRM may have lower RMSEs than CarbonTracker because CarbonTracker estimates less photosynthesis to occur at 00:00 and 12:00 UST than estimated by PolarVPRM. Arctic regions receive sunlight continuously through the mid-summer season, and Arctic tundra vegetation has been observed to conduct photosynthesis continuously throughout midsummer, despite low light levels and low temperatures found at solar midnight (Tieszen, 1973; Patankar et al., 2013). PolarVPRM's ability to simulate photosynthesis according to actual light availability at high latitudes therefore allows estimates of NEE to agree closely with averaged EC NEE, especially when considered at monthly intervals. In summary, PolarVPRM provides a simple approach for generating reliable estimates of NEE.

3.4 Regional trends (2001–2012)

Regional trends are examined here for the purpose of examining general tendencies in inter-annual variability, as uncertainties in regional-scale estimates of North American NEE limit the capacity to accurately quantify high-latitude regional-scale C balances. Model estimates of the mean annual carbon balance of the North American region north of 55° N indicate that this region may have been a carbon source from 2001–2004 and 2010–2012,

and a weak carbon sink between 2005–2009 (Fig. 5). Between 2001–2009, respiration diminished, and then rose again from 2010 onward. After 2004, GEE became less negative over time, indicating less CO_2 uptake per year. Respiration changes more than GEE over time, and appears to have a larger role in determining changes over time in NAHL net C uptake than photosynthesis.

Several general tendencies appear when examining monthly average NEE over time (2001–2012) from each PolarVPRM vegetation class (Fig. 6). In 2001–2005, PolarVPRM estimates that high-latitude North America was a carbon source (Fig. 5) as the source strength of tundra regions exceeded the sink strength of forested regions. Over time (2005–2010), forested regions took up less carbon through photosynthesis year after year (Fig. 6). Graminoid tundra and barren regions continue to function as net carbon sources, and forested regions continue to function as net carbon sinks. Shrub tundra regions appear to be shifting towards becoming carbon sinks because of an increase in the amount of C taken up through photosynthesis. The decrease in respiration observed in Fig. 5 is due largely to a small decrease in snow season respiration. Although this decrease is minor on a monthly level, its cumulative impact on the carbon balance is substantial. Forests have stronger fluxes than tundra vegetation, and therefore have a greater relative contribution to the North American high-latitude carbon cycle than tundra regions, leading to a net increase in CO_2 efflux from 2007 onward (Fig. 5).

3.5 Per-pixel trends (2001–2012)

Previous studies have described the influence of warming air temperatures on inducing increased rates of net carbon uptake by vegetation near the shrub and tree lines (Hinzman et al., 2005; Tape et al., 2006), and on increasing rates of CO_2 efflux (Schuur et al., 2009; Tarnocai, 2006). Remote sensing studies have found trends towards increased growing season length (Zeng et al., 2011), increased NDVI over tundra regions due to warming (Stow et al., 2004), and diminished NDVI over boreal regions due to reduced rates of photosynthesis (Verbyla, 2008). Since PolarVPRM is driven by remote sensing observations, the

effects of these environmental changes for HL carbon cycling can be examined by analyzing trends in PolarVPRM output.

Trends over time in carbon cycle variables were examined for each pixel in NAHL individually using the non-parametric Theil-Sen estimator (Sen's slope). Initial analyses were conducted according to mean annual values of net carbon uptake, NEE, respiration, and GEE (Fig. 7). Visual examination of these plots indicated a net increase in carbon efflux from high-latitude regions, focused mainly in forested regions (Fig. 7a). The observed increase in annual carbon efflux from forested regions over time arises mostly due to a decrease over time in the photosynthetic uptake of carbon (represented by an increase in GEE) (Fig. 7c). Although photosynthetic uptake in parts of northern Alaska and the Yukon increased over time, greater uptake was outweighed by the declines observed over forested regions. The net change in GEE is therefore mainly indicative of diminished sink strength over time. Effluxes of CO_2 from Arctic tundra regions increased over time due to greater rates of respiration (Fig. 7b). Overall, this results in a slight trend toward less net CO_2 uptake across the entire model domain (Fig. 7a), especially from 2005 onward.

The amount of carbon taken up by vegetation through photosynthesis increased over tundra regions, and declined sharply over forest regions (Fig. 7c). When considering trends only over the active growing season (when GEE < 0), there was a slight increase in the amount of carbon taken up by North American vegetation during the growing season (Fig. 8a). This discrepancy is due to the inability of model vegetation to conduct photosynthesis when temperatures rise above the maximum air temperatures permitted for photosynthesis, and due to increased drought stress in warm conditions. As air temperatures warm above the physiologically optimal temperatures, and drought stress increases, the capacity for photosynthesis diminishes strongly.

Positive air temperature anomalies and increased drought stress during the growing season therefore limit the total amount of carbon taken up by forest vegetation, while generally, rising EVI (Fig. 8c) and air temperatures (Fig. 8d) increase photosynthetic activity whenever temperatures are not excessively hot. It is also interesting to note that a further consequence of rising air temperatures is a concurrent rise in growing season rates of respira-

tion (Fig. 8b), which seems to partially counteract the increase in photosynthesis observed across the model domain (Fig. 8a).

Cooling trends in snow season NARR T_{air} resulted in colder T_{soil} over time south of the treeline, resulting in diminished respiration, but less change over time was observed in soil and air temperatures north of the treeline (Fig. 9c and d). Recent studies have indicated cooling trends in winter air temperatures over high-latitude regions of North America could be due to trends in the Madden–Julian Oscillation (Yoo et al., 2011), or due to deepened Eurasian snow depth (Cohen et al., 2012). As snow season length also diminishes over time (Fig. 9b), it could be expected that subnivean effluxes of CO_2 would contribute less carbon annually to the atmosphere over time. Only a small decline over time was observed in snow season respiration over forested regions (Fig. 9a). Conversely, diminished snow season length could contribute to the observed rises in growing season respiration (Fig. 8b). The initial decline, and later rise, in respiration are therefore likely to occur due to counteracting trends over time in snow and growing season respiration.

The boreal forest appears to have a dominant role in determining fluxes of CO_2 over North American latitudes north of 55° N. Although photosynthetic uptake in tundra regions increases over time, this is largely outweighed by concurrent rises in respiration due to warming air temperatures. Forest regions are also capable of greater rates of photosynthesis during the active growing season (GEE < 0), but carbon uptake is limited due to drought and temperature stress. As a result, reductions over time occur in the amount of carbon taken up by vegetation. Furthermore, although subnivean effluxes of CO_2 diminish over time due to shortened snow seasons and diminished snow season soil temperatures, annual rates of respiration increase over time. PolarVPRM simulations indicate that it is likely that North American HL regions have recently been emitting more CO_2 into the atmosphere in response to warming air temperatures.

4 Conclusions

PolarVPRM provides a remote-sensing based approach for generating high-resolution estimates of NEE using a parsimonious model approach that is specifically adapted for high-latitude regions. PolarVPRM adequately simulates high-latitude NEE by using Arctic-specific vegetation classes, and calculating snow and growing season R separately using soil and air temperatures, respectively. When PolarVPRM, CarbonTracker, and FLUXNET MTE were all examined against EC NEE averaged over three-hourly, daily and monthly timescales, the smallest RMSE values for each timescale were found in comparisons of PolarVPRM NEE to EC NEE, indicating reasonable model performance.

Due to the parsimonious model structure used in PolarVPRM, and the easily describable associations between inputs and outputs, examination of trends in PolarVPRM NEE and its drivers provides insights into how the NAHL carbon cycle may be responding to changing environmental conditions. PolarVPRM estimates of high-latitude (55–83° N) North American NEE showed an increase over time (2007–2012) in net carbon efflux by high-latitude ecosystems, and shifted recently between being a carbon sink (2005–2010), and carbon sink (2001–2004, 2011–2012). Initially, high-latitude regions increased their net uptake of carbon over time (2001–2005) due to an increase in rates of photosynthesis by Arctic vegetation. Subsequently, net carbon efflux from high-latitude regions increased (2011–2012) due to declines in photosynthesis over boreal regions in response to temperature and drought stress. Overall, PolarVPRM indicates that warmer air temperatures are enabling Arctic vegetation to take up more carbon photosynthetically, while simultaneously increasing high-latitude rates of respiration, and diminishing photosynthetic uptake of carbon by boreal vegetation.

Code availability

Model estimates of PolarVPRM NEE, respiration and GEE across North America (north of 55° N) will be made publicly available upon publication of this article. Code will be available by request from kluus@bgc-jena.mpg.de.

Appendix A: MODIS and NARR input data

Several changes were made to the remote-sensing derived input data used by PolarVPRM, relative to VPRM. Firstly, MODIS MOD10A2 observations of fractional snow cover (Hall et al., 1995; Hall and Riggs, 2007; Riggs and Hall, 2011) were included to differentiate snow and growing season respiration. Preliminary assessment indicated that the MOD10A2 Collection 5 fractional snow cover area has false positive and false negative values at high-latitude sites. False negatives in MODIS estimates of fractional snow cover occur when reflectance is very low in winter due to surface features or illumination factors. Omission errors can also arise during snowmelt over terrestrial pixels containing a mix of snow/ice and land, as land can warm up quickly, and be identified as snow-free when it exceeds the algorithm's temperature threshold (> 283 K) (G. Riggs, personal communication, 2012). False positives in MODIS SCA arise when the MODIS cloud mask misses a cloud or the edge of a cloud. Both false positives and false negatives are most common at high-latitude sites, due to the characteristic cloud cover, and low winter solar angles. These errors will be reduced in upcoming versions of MOD10 snow cover area (G. Riggs, personal communication, 2012).

In order to use MOD10A2 observations effectively, some filtering and smoothing techniques were applied to the remote-sensing observations before they were included in PolarVPRM. First, MOD10A2 observations were only used for pixels and time periods where both MOD10A2 and the corresponding surface reflectance observations were flagged as "excellent". Soil temperature masks were also applied to eliminate false positives in mid-summer, and false negatives in mid-winter. Furthermore, since snow melt and snow onset occur rapidly in high-latitude regions, the R `loess` (local polynomial regression fitting) smoothing algorithm (R Development Core Team, 2011) was applied to reduce noise in estimates of fractional snow cover, and to allow temporal gap filling for missing observations. When MODIS MOD10A2 observations were corrected using this approach, good agreement was then found between remotely sensed and locally observed fractional snow cover.

The original VPRM calculated LSWI and EVI from MOD09 surface reflectance. However, EVI calculated from MOD09 contained anomalous values at high latitude sites, likely due to

the prevalence of cloud cover and snow/ice, which have high reflectance of blue light, and therefore cause atmospheric over-correction. The MOD13 series of products provide more reliable estimates of EVI at high latitude sites, because a backup two-band EVI algorithm is used when blue band reflectance is high Solano et al. (2010). MOD13A1 EVI was therefore included in PolarVPRM instead of estimates of EVI calculated from MOD09A1 surface reflectance.

Meteorological observations from the North American Regional Reanalysis (NARR) were used to drive PolarVPRM. High-latitude meteorological estimates tend to be biased towards overestimating shortwave radiation due to errors in simulating both the amount of cloud cover, as well as the influence of clouds on the surface energy balance Walsh et al. (2009). It was therefore important that meteorological products with the smallest errors possible would be used as inputs to PolarVPRM. The selection process through which NARR was chosen involved comparing two well-established meteorological reanalysis products, NARR Mesinger et al. (2006) and the North American Land Data Assimilation System (NLDAS) Mitchell et al. (2004), to ground-based meteorological observations collected at Daring Lake, NWT Humphreys and Lafleur (2011); Lafleur and Humphreys (2008). Daring Lake was selected as the validation site for these products because it is less likely that the inputs to the NARR and NLDAS data assimilations had been extensively calibrated at Daring Lake, relative to the other sites, which are all Alaskan Ameriflux sites. Comparisons at Daring Lake indicated that although both NARR and NLDAS overestimated air temperatures at 2 m above ground (T_{air}) and downward shortwave radiation, these overestimates were much smaller in NARR. Furthermore, NARR has been used and validated in a number of high-latitude studies (e.g Langlois et al., 2012; Miller et al., 2014).

Errors and biases in NARR meteorological estimates at all year-round calibration and validation were examined by comparing NARR estimates to ground-based meteorological observations of soil temperature, air temperature and shortwave radiation. Results indicated relatively good agreement between measured and estimated soil/air temperatures ($R^2 \approx 0.9$) and shortwave radiation ($R^2 \approx 0.8$) across year-round calibration and validation sites, relative to products such as NLDAS and GLDAS.

NARR estimates of downward shortwave radiation, T_{air} at 2 m and soil temperature at 0–10 cm (T_{soil}) were therefore incorporated into PolarVPRM. In the error analysis (Sect. 3.2), biases in NARR inputs were assessed, along with their contributions to errors in NEE. Similarly, in the validation at high-latitude Canadian sites (Sect. 3.1), model errors were examined in relation to biases in NARR estimates, which are much more substantial at these high-latitude, remote Canadian sites than in Alaska. Overall, NARR shortwave radiation, air temperature and soil temperature, as well as MODIS EVI, LSWI and fractional snow cover area, are presently the best available inputs for high-latitude sites.

Acknowledgements. Funding for this research was provided through a Vanier Canada Graduate Scholarship (KAL). Data from the Canadian sites (DL, lh, cb, pi, and iq) was provided by P. Lafleur and E. Humphreys and collected by Lafleur and Humphreys, V. St. Louis, L. Poissant, J. Barker, and M. Pilote. Funding and support was provided by the Canadian Foundation for Climate and Atmospheric Sciences, the Natural Science and Engineering Research Council, the Canadian International Polar Year Program and the Polar Continental Shelf Project. Data from Imnavait, Alaska were provided by E. Euskirchen, C. Edgar, and M. S. Bret-Harte and collected through a grant from the National Science Foundation, "Collaborative Research on Carbon, Water, and Energy Balance of the Arctic Landscape at Flagship Observatories in Alaska and Siberia". Data from Ivotuk and Atqasuk was generously provided by W. Oechel and his group. The authors wish to thank Martin Jung for providing FLUXNET MTE output. CarbonTracker CT2011_oi results were provided by NOAA ESRL, Boulder, Colorado, USA. The authors also wish to thank R. E. J. Kelly and C. R. Duguay for providing valuable input and advice.

The service charges for this open-access publication
have been covered by the Max Planck Society.

References

Aurela, M., Laurila, T., and Tuovinen, J.: The timing of snow melt controls the annual CO_2 balance in a subarctic fen, Geophys. Res. Lett., 31, L16119, doi:10.1029/2004GL020315, 2004.

Barr, A., Black, T., Hogg, E., Kljun, N., Morgenstern, K., and Nesic, Z.: Inter-annual variability in the leaf area index of a boreal aspen-hazelnut forest in relation to net ecosystem production, Agr. Forest Meteorol., 126, 237–255, 2004.

Belshe, E., Schuur, E., and Bolker, B.: Tundra ecosystems observed to be CO_2 sources due to differential amplification of the carbon cycle, Ecol. Lett., 16, 1316–1324, doi:10.1111/ele.12164, 2013.

Bernacchi, C., Bagley, J., Serbin, S., Ruiz-Vera, U., Rosenthal, D., and Vanloocke, A.: Modelling C3 photosynthesis from the chloroplast to the ecosystem, Plant. Cell Environ., 36, 1641–1657, doi:10.1111/pce.12118, 2013.

Bliss, L.: Seed germination in arctic and alpine species, Arctic, 11, 180–188, 1958.

Bondeau, A., Smith, P. C., Zaehle, S., Schaphoff, S., Lucht, W., Cramer, W., Gerten, D., Lotze-Campen, H., Müller, C., Reichstein, M., and Smith, B.: Modelling the role of agriculture for the 20th century global terrestrial carbon balance, Glob. Change Biol., 13, 679–706, 2007.

Chapin III, F. S.:Direct and indirect effects of temperature on arctic plants, Polar Biology, 2, 47–52, 1983.

Chapin III, F. and Shaver, G.: Individualistic growth response of tundra plant species to environmental manipulations in the field, Ecology, 66, 564–576, 1985.

Chapin III, F. S., Eugster, W., McFadden, J. P., Lynch, A. H., and Walker, D. A.: Summer differences among arctic ecosystems in regional climate forcing, J. Climate, 13, 2002–2010, 2000.

Cohen, J. L., Furtado, J. C., Barlow, M. A., Alexeev, V. A., and Cherry, J. E.: Arctic warming, increasing snow cover and widespread boreal winter cooling, Environ. Res. Lett., 7, 014007, 2012.

Dietze, M., Serbin, S., Davidson, C., Desai, A., Feng, X., Kelly, R., Kooper, R., LeBauer, D., Mantooth, J., McHenry, K., and Wang, D.: A quantitative assessment of a terrestrial biosphere model's data needs across North American biomes, J. Geophys. Res.-Biogeo., 119, 286–300, doi:10.1002/2013JG002392, 2014.

Elberling, B.: Annual CO_2 effluxes in the High Arctic: the role of snow and vegetation type, Soil Biol. Biochem., 39, 646–654, 2007.

Elberling, B. and Brandt, K.: Uncoupling of microbial CO_2 production and release in frozen soil and its implications for field studies of arctic C cycling, Soil Biol. Biochem., 35, 263–272, 2003.

Euskirchen, E., Bret-Harte, M., Scott, G., Edgar, C., and Shaver, G.: Seasonal patterns of carbon dioxide and water fluxes in three representative tundra ecosystems in northern Alaska, Ecosphere, 3, 1–19, 2012.

Fisher, J. B., Sikka, M., Oechel, W. C., Huntzinger, D. N., Melton, J. R., Koven, C. D., Ahlström, A., Arain, M. A., Baker, I., Chen, J. M., Ciais, P., Davidson, C., Dietze, M., El-Masri, B., Hayes, D., Huntingford, C., Jain, A. K., Levy, P. E., Lomas, M. R., Poulter, B., Price, D., Sahoo, A. K., Schaefer, K., Tian, H., Tomelleri, E., Verbeeck, H., Viovy, N., Wania, R., Zeng, N., and Miller, C. E.: Carbon cycle uncertainty in the Alaskan Arctic, Biogeosciences, 11, 4271–4288, doi:10.5194/bg-11-4271-2014, 2014.

Gold, W. and Bliss, L.: Water limitations and plant community development in a polar desert, Ecology, 76, 1558–1568, 1995.

Goulden, M. L., Munger, J. W., Fan, S.-M., Daube, B. C., and Wofsy, S. C.: Measurements of carbon sequestration by long-term eddy covariance: methods and a critical evaluation of accuracy, Glob. Change Biol., 2, 169–182, 1996.

Grace, J., Nichol, C., Disney, M., Lewis, P., Quaife, T., and Bowyer, P.: Can we measure terrestrial photosynthesis from space directly using spectral reflectance and fluorescence, Glob. Change Biol., 13, 1484–1497, doi:10.1111/j.1365-2486.2007.01352.x, 2007.

Grogan, P. and Jonasson, S.: Ecosystem CO_2 production during winter in a Swedish subartic region: the relative importance of climate and vegetation type, Glob. Change Biol., 12, 1479–1495, 2006.

Hall, D. and Riggs, G.: Accuracy assessment of the MODIS snow products, Hydrol. Process., 21, 1534–1547, 2007.

Hall, D., Riggs, G., and Salomonson, V.: Development of methods for mapping global snow cover using moderate resolution imaging spectroradiometer data, Remote Sens. Environ., 54, 127–140, 1995.

Harazono, Y., Mano, M., Miyata, A., Zulueta, R. C., and Oechel, W. C.: Inter-annual carbon dioxide uptake of a wet sedge tundra ecosystem in the Arctic, Tellus B, 55, 215–231, 2003.

Heim, B., Bartsch, A., Elger, K., Lantuit, H., Boike, J., Muster, S., Langer, M., Duguay, C., Hachem, S., Soliman, A., Paulik, C., Strozzi, T., and Seifert, F.: ESA DUE Permafrost: an Earth observation (EO) permafrost monitoring system, EARSeL eProceedings, 10, 73–82, 2011.

Hilker, T., Coops, N., Wulder, M., Black, T., and Guy, R.: The use of remote sensing in light use efficiency based models of gross primary production: a review of current status and future requirements, Sci. Total Environ., 404, 411–423, doi:10.1016/j.scitotenv.2007.11.007, 2008.

Hinzman, L., Bettez, N., Bolton, W., Chapin, F., Dyurgerov, M., Fastie, C., Griffith, B., Hollister, R., Hope, A., Huntington, H., Jensen, A., Jia, G., Jorgenson, T., Kane, D., Klein, D., Kofinas, G., Lynch, A., Lloyd, A., McGuire, A. D., Nelson, F., Oechel, W., Osterkamp, T., Racine, C., Romanovsky, V., Stone, R., Stow, D., Sturm, M., Tweedie, C., Vourlitis, G., Walker, M., Walker, D., Webber, P., Welker, J., Winker, K., and Yoshikawa, K.: Evidence and implications of recent climate change in northern Alaska and other arctic regions, Climatic Change, 72, 251–298, 2005.

Hollister, R. D., Webber, P. J., and Tweedie, C. E.: The response of Alaskan arctic tundra to experimental warming: differences between short-and long-term responses, Glob. Change Biol., 11, 525–536, 2005.

Huemmrich, K., Gamon, J., Tweedie, C., Oberbauer, S., Kinoshita, G., Houston, S., Kuchy, A., Hollister, R., Kwon, H., Mano, M., Harazono, Y., Webber, P. J., and Oechel, W. C.: Remote sensing of tundra gross ecosystem productivity and light use efficiency under varying temperature and moisture conditions, Remote Sens. Environ., 114, 481–489, 2010.

Humphreys, E. and Lafleur, P.: Does Earlier Snowmelt Lead to Greater CO_2 Sequestration in Two Low Arctic Tundra Ecosystems?, Vol. 38, 2011.

Johnson, D. and Caldwell, M.: Gas exchange of four arctic and alpine tundra plant species in relation to atmospheric and soil moisture stress, Oecologia, 21, 93–108, 1975.

Jung, M., Henkel, K., Herold, M., and Churkina, G.: Exploiting synergies of global land cover products for carbon cycle modeling, Remote Sens. Environ., 101, 534–553, 2006.

Jung, M., Reichstein, M., and Bondeau, A.: Towards global empirical upscaling of FLUXNET eddy covariance observations: validation of a model tree ensemble approach using a biosphere model, Biogeosciences, 6, 2001–2013, doi:10.5194/bg-6-2001-2009, 2009.

Krol, M., Houweling, S., Bregman, B., van den Broek, M., Segers, A., van Velthoven, P., Peters, W., Dentener, F., and Bergamaschi, P.: The two-way nested global chemistry-transport zoom model TM5: algorithm and applications, Atmos. Chem. Phys., 5, 417–432, doi:10.5194/acp-5-417-2005, 2005.

Kwon, H.-J., Oechel, W. C., Zulueta, R. C., and Hastings, S. J.: Effects of climate variability on carbon sequestration among adjacent wet sedge tundra and moist tussock tundra ecosystems, J. Geophys. Res.-Biogeo., 111, G03014, doi:10.1029/2005JG000036, 2006.

Lafleur, P. and Humphreys, E.: Spring warming and carbon dioxide exchange over low Arctic tundra in central Canada, Glob. Change Biol., 14, 740–756, 2008.

Lafleur, P., Humphreys, E. R., St. Louis, V. L., Myklebust, M. C., Papakyriakou, T., Poissant, L., Barker, J. D., Pilote, M., and Swystun, K.: Variation in peak growing season net ecosystem production across the Canadian Arctic, Environ. Sci. Technol., 46, 7971–7977, doi:10.1021/es300500m, 2012.

Langlois, A., Royer, A., Derksen, C., Montpetit, B., Dupont, F., and Goïta, K.: Coupling the snow thermodynamic model SNOWPACK with the microwave emission model of layered snowpacks for subarctic and arctic snow water equivalent retrievals, Water Resour. Res., 48, W12524, doi:10.1029/2012WR012133, 2012.

Larsen, K., Ibrom, A., Jonasson, S., Michelsen, A., and Beier, C.: Significance of cold-season respiration and photosynthesis in a subarctic heath ecosystem in Northern Sweden, Glob. Change Biol., 13, 1498–1508, doi:10.1111/j.1365-2486.2007.01370.x 2007.

Laskowski, C.: Seasonal, annual, and interannual carbon dynamics of a remote tussock tundra ecosystem in Ivotuk, Alaska, PhD thesis, University of California Davis and San Diego State University, 2010.

Lin, J., Pejam, M., Chan, E., Wofsy, S., Gottlieb, E., Margolis, H., and McCaughey, J.: Attributing uncertainties in simulated biospheric carbon fluxes to different error sources, Global Biogeochem. Cy., 25, GB2018, doi:10.1029/2010GB003884, 2011.

Loranty, M. M., Goetz, S. J., Rastetter, E. B., Rocha, A. V., Shaver, G. R., Humphreys, E. R., and Lafleur, P. M.: Scaling an instantaneous model of tundra NEE to the Arctic landscape, Ecosystems, 14, 76–93, 2011.

Luus, K., Kelly, R., Lin, J., Humphreys, E., Lafleur, P., and Oechel, W.: Modeling the influence of snow cover on low Arctic net ecosystem exchange, Environ. Res. Lett., 8, 035045, doi:10.1088/1748-9326/8/3/035045, 2013a.

Luus, K. A., Gel, Y., Lin, J. C., Kelly, R. E. J., and Duguay, C. R.: Pan-Arctic linkages between snow accumulation and growing-season air temperature, soil moisture and vegetation, Biogeosciences, 10, 7575–7597, doi:10.5194/bg-10-7575-2013, 2013b.

Luus, K., Lin, J., Kelly, R., and Duguay, C.: Subnivean Arctic and sub-Arctic net ecosystem exchange (NEE): towards representing snow season processes in models of NEE using cryospheric remote sensing, Prog. Phys. Geog., 37, 484–515, doi:10.1177/0309133313491130, 2013c.

Mahadevan, P., Wofsy, S., Matross, D., Xiao, X., Dunn, A., Lin, J., Gerbig, C., Munger, J., Chow, V., and Gottlieb, E.: A satellite-based biosphere parameterization for net ecosystem CO_2 exchange: Vegetation Photosynthesis and Respiration Model (VPRM), Global Biogeochem. Cy., 22, GB2005, doi:10.1029/2006GB002735, 2008.

Marchetto, A.: rkt: Mann–Kendall test, Seasonal and Regional Kendall Tests, available at: http://CRAN.R-project.org/package=rkt (last access: 1 March 2013), R package version 1.1, 2012.

Masarie, K., Pétron, G., Andrews, A., Bruhwiler, L., Conway, T., Jacobson, A., Miller, J., Tans, P., Worthy, D., and Peters, W.: Impact of CO_2 measurement bias on CarbonTracker surface flux estimates, J. Geophys. Res., 116, D17305, doi:10.1029/2011JD016270, 2011.

McGuire, A. D., Macdonald, R., Schuur, E., Harden, J., Kuhry, P., Hayes, D., Christensen, T., and Heimann, M.: The carbon budget of the northern cryosphere region, Current Opinion in Environmental Sustainability, 2, 231–236, 2010.

Mesinger, F., DiMego, G., Kalnay, E., Mitchell, K., Shafran, P. C., Ebisuzaki, W., Jovic, D., Woollen, J., Rogers, E., Berbery, E. H., Michael B. Ek, M., Fan, Y., Grumbine, R., Higgins, W., Li, H., Lin, Y., Manikin, G., Parrish, D., Shi, W.: North American regional reanalysis, B. Am. Meteorol. Soc., 87, 343–360, 2006.

Miller, C. E. and Dinardo, S. J.: CARVE: the carbon in arctic reservoirs vulnerability experiment, in: Aerospace Conference, 2012 IEEE, 1–17, IEEE, 2012.

Miller, P.: Environmental and vegetational variation across a snow accumulation area in montane tundra in central Alaska, Ecography, 5, 85–98, 2006.

Miller, S. M., Worthy, D. E., Michalak, A. M., Wofsy, S. C., Kort, E. A., Havice, T. C., Andrews, A. E., Dlugokencky, E. J., Kaplan, J. O., Levi, P. J., Tian, H., and Zhang, B.: Observational constraints on the distribution, seasonality, and environmental predictors of North American boreal methane emissions, Global Biogeochem. Cy., 28, 146–160, doi:10.1002/2013GB004580, 2014.

Mitchell, K. E., Lohmann, D., Houser, P. R., Wood, E. F., Schaake, J. C., Robock, A., Cosgrove, B. A., Sheffield, J., Duan, Q., Luo, L., Higgins, R., Pinker, R., Tarpley, J., Lettenmaier, D., Marshall, C., Entin, J., Pan, M., Shi, W., Koren, V., Meng, J., Ramsay, B., and Bailey, A.: The multi-institution North American Land Data Assimilation System (NLDAS): Utilizing multiple GCIP products and partners in a continental distributed hydrological modeling system, J. Geophys. Res.-Atmos., 109, D07S90, doi:10.1029/2003JD003823, 2004.

Morgner, E., Elberling, B., Strebel, D., and Cooper, E.: The importance of winter in annual ecosystem respiration in the High Arctic: effects of snow depth in two vegetation types, Polar Res., 29, 58–74, 2010.

Oberbauer, S. and Miller, P.: Plant water relations in montane and tussock tundra vegetation types in Alaska, Arctic Alpine Res., 11, 69–81, 1979.

Oberbauer, S. F. and Dawson, T. E.: Water relations of Arctic vascular plants, in: Arctic Ecosystems in a Changing Climate: An Ecophysiological Perspective, Academic Press Inc, San Diego, USA, 259–279, 1992.

Oechel, W. C., Vourlitis, G. L., Hastings, S. J., and Bochkarev, S. A.: Change in Arctic CO_2 flux over two decades: effects of climate change at Barrow, Alaska, Ecol. Appl., 5, 846–855, 1995.

Olsson, P., Sturm, M., Racine, C., Romanovsky, V., and Liston, G.: Five stages of the Alaskan Arctic cold season with ecosystem implications, Arct. Antarct. Alp. Res., 35, 74–81, 2003.

Panikov, N., Flanagan, P., Oechel, W., Mastepanov, M., and Christensen, T.: Microbial activity in soils frozen to below $-39\,^{\circ}C$, Soil Biol. Biochem., 38, 785–794, 2006.

Patankar, R., Mortazavi, B., Oberbauer, S. F., and Starr, G.: Diurnal patterns of gas-exchange and metabolic pools in tundra plants during three phases of the arctic growing season, Ecology and Evolution, 3, 375–388, doi:10.1002/ece3.467, 2013.

Peters, W., Jacobson, A. R., Sweeney, C., Andrews, A. E., Conway, T. J., Masarie, K., Miller, J. B., Bruhwiler, L. M., Petron, G., Hirsch, A. I., Worthy, D., van der Werf, G., Randerson, J., Wennberg, P., Krol, M., and Tans, P.: An atmospheric perspective on North American carbon dioxide exchange: CarbonTracker, P. Natl. Acad. Sci. USA, 104, 18925–18930, 2007.

Potter, C., Randerson, J., and Field, C. B.: Terrestrial ecosystem production: a process model based on global satellite and surface data, Global Biogeochemical Models, 7, 811–841, 1993.

R Development Core Team: R: a Language and Environment for Statistical Computing, R Foundation for Statistical Computing, Vienna, Austria, available at: http://www.R-project.org/ (last access: 29 January 2015), ISBN 3-900051-07-0, 2011.

Riggs, G. and Hall, D.: MODIS snow and ice products, and their assessment and applications, in: Land Remote Sensing and Global Environmental Change, Remote Sensing and Digital Image Processing, edited by: Ramachandran, B., Justice, C. O., and Abrams, M. J., 11, 681–707, 2011.

Schaefer, K., Zhang, T., Bruhwiler, L., and Barrett, A.: Amount and timing of permafrost carbon release in response to climate warming, Tellus B, 63, 165–180, 2011.

Schuur, E., Vogel, J., Crummer, K., Lee, H., Sickman, J., and Osterkamp, T.: The effect of permafrost thaw on old carbon release and net carbon exchange from tundra, Nature, 459, 556–559, 2009.

Sen, P. K.: Estimates of the regression coefficient based on Kendall's tau, J. Am. Stat. Assoc., 63, 1379–1389, 1968.

Shaver, G., Chapin III, F., and Gartner, B.: Factors limiting seasonal growth and peak biomass accumulation in Eriophorum vaginatum in Alaskan tussock tundra, J. Ecol., 74, 257–278, 1986.

Shaver, G., Street, L., Rastetter, E., Van Wijk, M., and Williams, M.: Functional convergence in regulation of net CO_2 flux in heterogeneous tundra landscapes in Alaska and Sweden, J. Ecol., 95, 802–817, 2007.

Shaver, G., Rastetter, E., Salmon, V., Street, L., van de Weg, M., Rocha, A., van Wijk, M., and Williams, M.: Pan-Arctic modelling of net ecosystem exchange of CO_2, Philos. T. R. Soc. B, 368, 20120485, doi:10.1098/rstb.2012.0485, 2013.

Solano, R., Didan, K., Jacobson, A., and Huete, A.: MODIS Vegetation Indices (MOD13) C5 User's Guide, Terrestrial Biophysics and Remote Sensing Lab, The University of Arizona, available at: http://www.ctahr.hawaii.edu/grem/modis-ug.pdf (last access: 29 January 2015), 2010.

Stow, D., Hope, A., McGuire, D., Verbyla, D., Gamon, J., Huemmrich, F., Houston, S., Racine, C., Sturm, M., Tape, K., Hinzman, L., Yoshikawa, K., Tweedie, C., Noyle, B., Silapaswan, C., Douglas, D., Griffith, B., Jia, G., Epstein, H., Walker, D., Daeschner, S., Petersen, A., Zhou, L., and Myneni, R.: Remote sensing of vegetation and land-cover change in Arctic Tundra Ecosystems, Remote Sens. Environ., 89, 281–308, 2004.

Stoy, P. C., Williams, M., Disney, M., Prieto-Blanco, A., Huntley, B., Baxter, R., and Lewis, P.: Upscaling as ecological information transfer: a simple framework with application to Arctic ecosystem carbon exchange, Landscape Ecol., 24, 971–986, 2009.

Sturm, M.: Snow distribution and heat flow in the Taiga, Arctic Alpine Res., 24, 145–152, 1992.

Sullivan, P., Welker, J., Arens, S., and Sveinbjörnsson, B.: Continuous estimates of CO_2 efflux from arctic and boreal soils during the snow-covered season in Alaska, J. Geophys. Res.-Biogeo., 113, G04009, doi:10.1029/2008JG000715, 2008.

Tape, K., Sturm, M., and Racine, C.: The evidence for shrub expansion in Northern Alaska and the Pan-Arctic, Glob. Change Biol., 12, 686–702, 2006.

Tarnocai, C.: The effect of climate change on carbon in Canadian peatlands, Global Planet. Change, 53, 222–232, 2006.

Thompson, C., McGuire, A., Clein, J., Chapin, F., and Beringer, J.: Net carbon exchange across the arctic tundra-boreal forest transition in Alaska 1981–2000, Mitigation and Adaptation Strategies for Global Change, 11, 805–827, 2006.

Tieszen, L.: Photosynthesis and respiration in arctic tundra grasses: field light intensity and temperature responses, Arctic Alpine Res., 5, 239–251, 1973.

Verbyla, D.: The greening and browning of Alaska based on 1982–2003 satellite data, Global Ecol. Biogeogr., 17, 547–555, 2008.

Walker, D., Raynolds, M., Daniëls, F., Einarsson, E., Elvebakk, A., Gould, W., Katenin, A., Kholod, S., Markon, C., Melnikov, E., Moskalenko, N., Talbot, S., Yurtsev, B., and The other members of the CAVM Team: The circumpolar Arctic vegetation map, J. Veg. Sci., 16, 267–282, 2005.

Walker, M., Walker, D., Welker, J., Arft, A., Bardsley, T., Brooks, P., Fahnestock, J., Jones, M., Losleben, M., Parsons, A., Seastedt, T., and Turner, P.: Long-term experimental manipulation of winter snow regime and summer temperature in arctic and alpine tundra, Hydrol. Process., 13, 2315–2330, 1999.

Walsh, J. E., Chapman, W. L., and Portis, D. H.: Arctic cloud fraction and radiative fluxes in atmospheric reanalyses, J. Climate, 22, 2316–2334, 2009.

Yoo, C., Feldstein, S., and Lee, S.: The impact of the Madden–Julian Oscillation trend on the Arctic amplification of surface air temperature during the 1979–2008 boreal winter, Geophys. Res. Lett., 38, L24804, doi:10.1029/2011GL049881, 2011.

Zeng, H., Jia, G., and Epstein, H.: Recent changes in phenology over the northern high latitudes detected from multi-satellite data, Environ. Res. Lett., 6, 045508, 2011.

Zimov, S., Semiletov, I., Daviodov, S., Voropaev, Y., Prosyannikov, S., Wong, C., and Chan, Y.: Wintertime CO_2 emission from soils of Northeastern Siberia, Arctic, 46, 197–204, 1993.

Table 1. PolarVPRM vegetation classes, created by combining and aggregating CAVM and SYNMAP vegetation classes. SYNMAP tree classes are described according to leaf type (broad, needle or mixed) followed by leaf longevity (evergreen, deciduous, or mixed), as in Jung et al. (2006).

Veg class	Source	Description
Evergreen forest	SYNMAP	Trees needle evergreen; trees broad evergreen; trees mixed evergreen
Deciduous forest	SYNMAP	Trees needle deciduous; trees needle mixed; trees broad deciduous; Trees broad mixed; trees mixed deciduous; trees mixed mixed
Mixed tree/grass/ shrub forest	SYNMAP	Trees and shrubs; trees and grasses; trees and crops; crops
Shrubland	SYNMAP	Shrubs; shrubs and crops
Shrub tundra	SYNMAP	Shrubs and barren
Shrub tundra	CAVM	Prostrate dwarf-shrub, herb tundra; erect dwarf-shrub tundra; Low-shrub tundra
Graminoid tundra	SYNMAP	Grasses; grasses and crops
Graminoid tundra	CAVM	Rush/grass, forb, cryptogam tundra; graminoid, prostrate dwarf-shrub, forb tundra; Prostrate/hemiprostrate dwarf-shrub tundra; nontussock sedge, dwarf-shrub, moss tundra; tussock-sedge, dwarf-shrub, moss tundra
Barren/wetland	SYNMAP	Grasses and barren; barren
Barren/wetland	CAVM	Cryptogam, herb barren; cryptogam barren complex (bedrock); Sedge/grass, moss wetland; sedge, moss, dwarf-shrub wetland; Sedge, moss, low-shrub wetland; noncarbonate mountain complex; Carbonate mountain complex

Table 2. Summary of meteorological and land surface remote sensing inputs to PolarVPRM.

Input	Source	Spatial resolution	Temporal resolution
Shortwave radiation ($W\,m^{-2}$)	NARR	0.3°	Three-hourly
Air temperature (° Kelvin)	NARR	0.3°	Three-hourly
Soil temperature (° Kelvin)	NARR	0.3°	Three-hourly
Fractional snow cover (%)	MODIS MOD10A2	500 m	Eight-day
Enhanced vegetation index (0–1)	MODIS MOD13A1	500 m	Sixteen-day
Land surface water index (0–1)	MODIS MOD09A1	500 m	Eight-day

Table 3. Calibration and validation sites for each vegetation type, years of data used, and locations. Calibration sites are bolded, and validation sites at which cold season EC observations were unavailable are italicized.

Vegetation type	Calibration site	Validation sites	Year	Latitude (°)	Longitude (°)
Shrub tundra	**Daring Lake (DL)**		2005	64.869	−111.575
Shrub tundra		*Cape Bounty (cb)*	2008	74.915	−109.574
Shrub tundra		*Lake Hazen (lh)*	2008	81.823	−71.381
Shrub tundra		*Iqaluit (iq)*	2008	63.7903	−68.560
Graminoid tundra	**Ivotuk (IV)**		2005	68.487	−155.748
Graminoid tundra		Imnavait (Im)	2008	68.606	−149.304
Graminoid tundra		*Pond Inlet (pi)*	2008	72.693	−77.958
Wetland/barren	**Atqasuk (AT)**		2005	70.470	−157.409
Wetland/barren		Barrow (Ba)	2001	71.323	−156.626

Table 4. MBE and RMSE (in µmol CO_2 m^{-2} s^{-1}) from comparisons of three-hourly PolarVPRM NEE, to July 2008 eddy covariance observations of NEE at four Canadian Arctic validation sites.

	Cape Bounty (cb)	Iqaluit (iq)	Lake Hazen (lh)	Pond Inlet (pi)	Mean
Root mean squared error (RMSE)	0.66	1.01	0.57	0.92	0.79
Mean bias error (MBE)	−0.33	0.15	0.39	−0.44	−0.23

Table 5. Error statistics (RMSE and MBE; in μmol $CO_2\,m^{-2}\,s^{-1}$) found through the comparison of monthly, daily, and 3-hourly averaged estimates of NEE from PolarVPRM, CarbonTracker and FLUXNET Model-Tree Ensemble relative to observations of three-hourly, daily and monthly averages of NEE from Atqasuk (AT), Barrow (Ba), Daring Lake (DL), Imnavait (Im) and Ivotuk (IV).

Resolution	Error	Model	AT	Ba	DL	Im	IV	Mean
Monthly	RMSE	PolarVPRM	0.42	0.93	0.42	1.61	0.59	0.79
Monthly	RMSE	CarbonTracker	0.57	0.48	0.92	1.58	0.86	0.88
Monthly	RMSE	FLUXNET MTE	1.10	1.13	1.40	2.14	1.19	1.39
Daily	RMSE	PolarVPRM	0.75	9.42	3.80	12.02	0.33	5.26
Daily	RMSE	CarbonTracker	2.87	4.74	6.21	10.83	2.90	5.51
3-hrly	RMSE	PolarVPRM	1.29	1.52	0.75	3.27	1.97	1.76
3-hrly	RMSE	CarbonTracker	1.61	1.20	2.20	4.45	2.91	2.47
Monthly	MBE	PolarVPRM	−0.14	−0.51	0.14	−1.15	0.02	−0.33
Monthly	MBE	CarbonTracker	0.03	−0.20	−0.37	−1.01	0.20	−0.27
Monthly	MBE	FLUXNET MTE	−0.64	−0.82	−1.03	−1.55	−0.43	−0.89
Daily	MBE	PolarVPRM	0.06	0.84	-0.38	1.37	-0.03	0.37
Daily	MBE	CarbonTracker	-0.22	0.42	-0.63	1.23	-0.23	0.12
3-hrly	MBE	PolarVPRM	−0.03	−0.65	0.23	−1.43	0.12	−0.35
3-hrly	MBE	CarbonTracker	0.26	−0.33	0.30	−1.27	0.42	−0.12

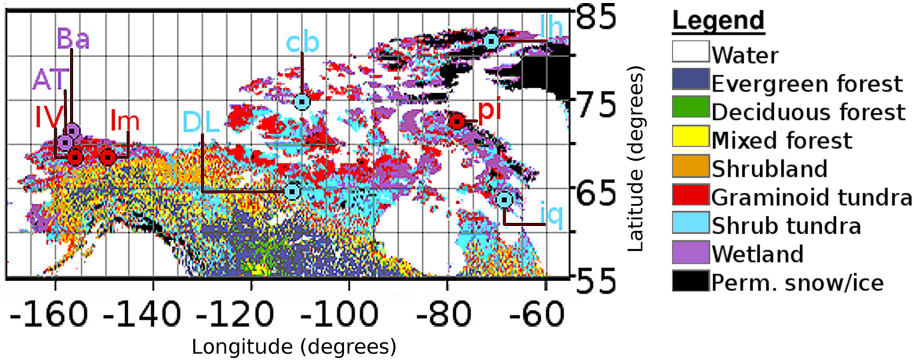

Figure 1. Map of all North American calibration and validation sites and their predominant vegetation types: graminoid tundra (red), shrub tundra (cyan) or wetland (purple). Calibration sites are indicated in all caps (e.g. AT), year-round validation sites are capitalized (e.g. Im), and growing season validation sites appear in lowercase (e.g. cb). For a summary of all study site locations, please refer to Table 3.

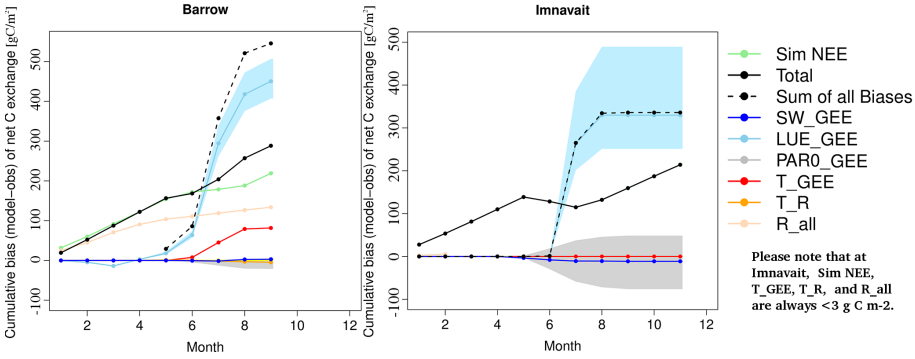

Figure 2. Cumulative monthly bias in PolarVPRM estimates of net C exchange at Barrow (left) and Imnavait (right), relative to eddy covariance observations at these sites. Errors in GEE are designated as being due to the associations between GEE and downward shortwave radiation (SW_GEE), GEE and light use efficiency (LUE_GEE), and of the parameter describing the association between GEE and PAR0 (PAR0_GEE). Shaded areas surrounding (PAR0_GEE) and (LUE_GEE) represent the range of biases possible from the determination of PAR0 and λ from eddy covariance observations. Total biases in temperature and GEE (T_GEE), and between temperature and respiration (T_R) are also described, along with the total biases in respiration (R_all) and NEE. Comparisons are shown for the range of months for which eddy covariance observations were acquired at Barrow in 2001 (January–September), and at Imnavait in 2008 (February–October).

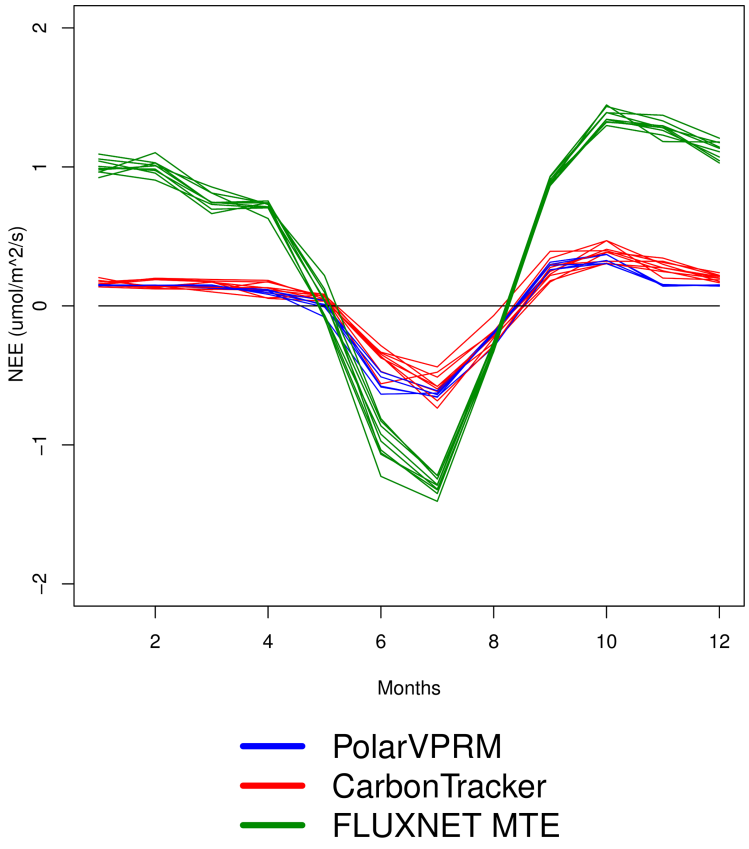

Figure 3. Monthly average NEE for high-latitude North America (north of 55° N from PolarVPRM (blue), FLUXNET MTE (green) and CarbonTracker (red). Average values are indicated for each year (2001–2009) individually.

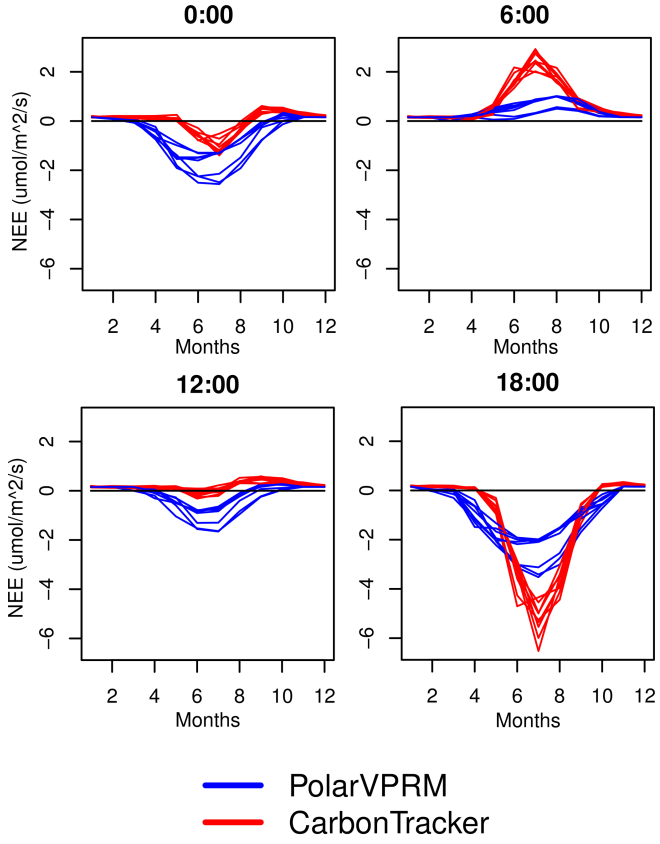

Figure 4. Spatially averaged North American high-latitude NEE from PolarVPRM (blue) and CarbonTracker (red). All estimates are averaged monthly at four distinct times of day, shown in Universal Time (UST) rather than according to local time zones.

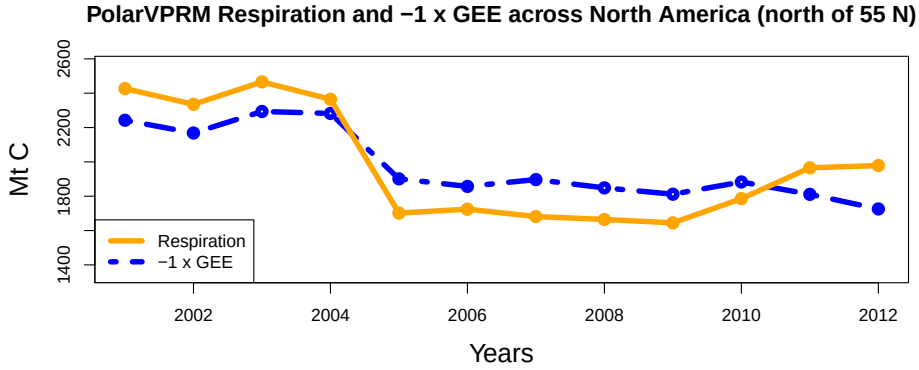

Figure 5. Relative contributions of PolarVPRM respiration and photosynthesis (GEE, plotted here as $-1\times$GEE) to inter-annual variability in the net C balance of the North American terrestrial region north of 55° N (NAHL).

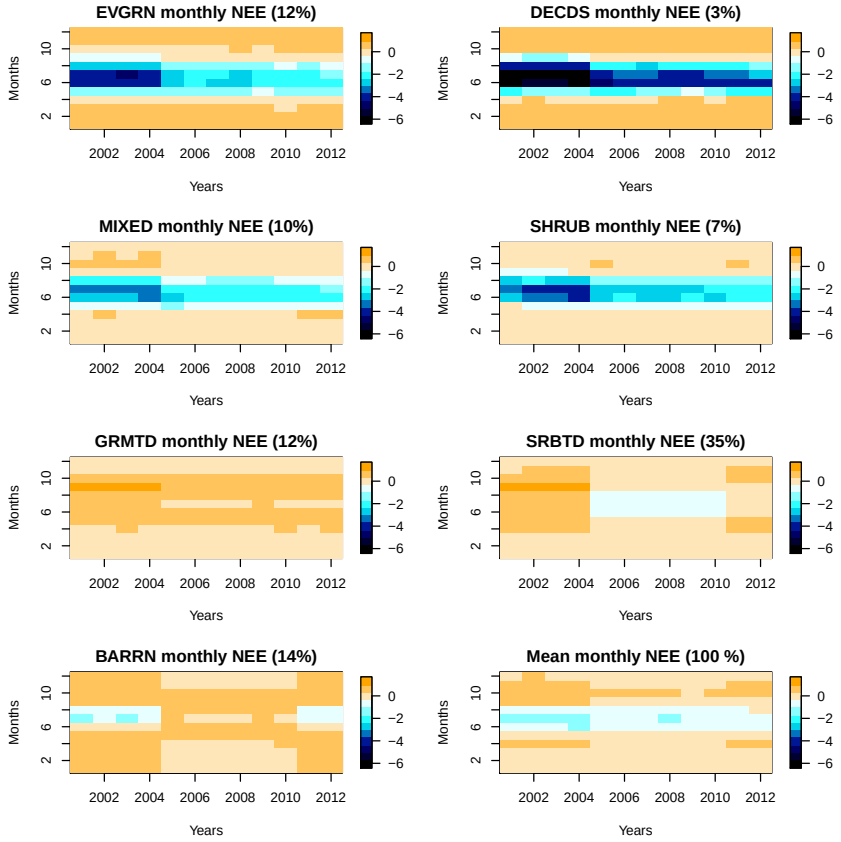

Figure 6. Average monthly NEE (in µmol CO_2 m^{-2} s^{-1}) for the entire North American region north of 55° N (Mean), as well as for seven vegetation classes within this region: deciduous forest (DECDS), evergreen forest (EVGRN), mixed forest (MIXED), shrub (SHRUB), graminoid tundra (GRMTD), shrub tundra (SRBTD), and barren/wetland (BARRN). The percentage of the model domain covered by each vegetation class is indicated in the title of each subplot.

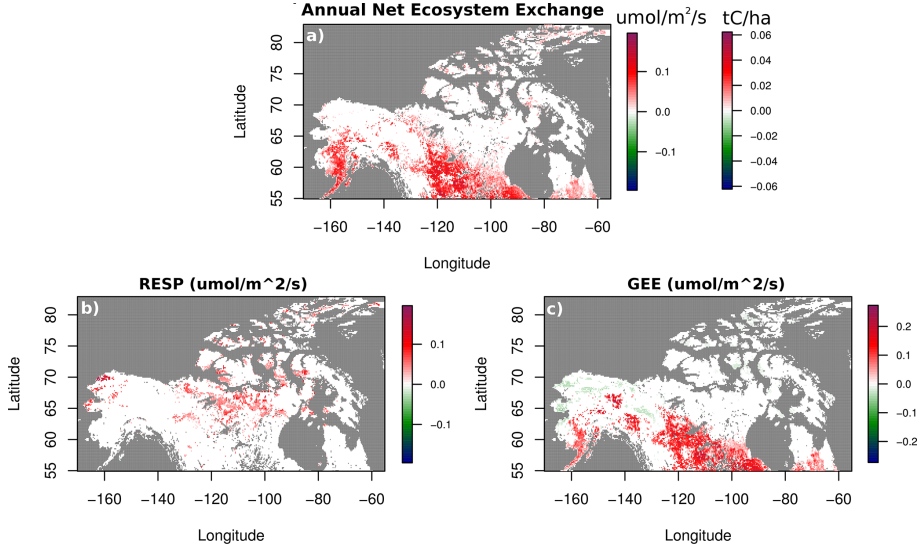

Figure 7. Sen's slope values, indicating the median change (2001–2012) in PolarVPRM estimates of mean annual NEE **(a)**, respiration **(b)** and GEE **(c)**. In **(a)**, changes over time in NEE are indicated in bothμmol CO_2 m^{-2} s^{-1} and tC ha^{-1} using the same colour scheme. All Sen's slope values shown correspond to p values < 0.05. Pixels with $>$50% fractional water content are indicated in grey. Please note that the negative sign convention in GEE has been maintained, meaning that a positive trend in GEE corresponds to diminished uptake of carbon through photosynthesis.

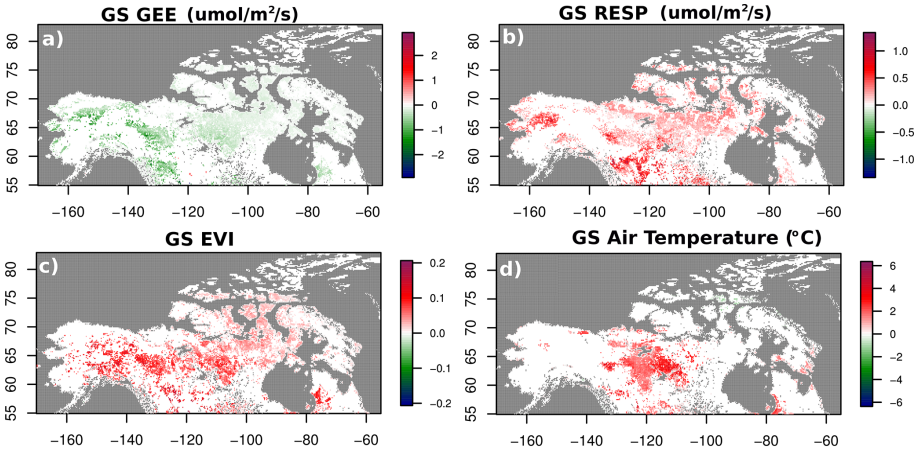

Figure 8. Sen's slope of median change (2001–2012) in PolarVPRM estimates of growing season carbon cycle variables, and driver data. All statistically significant (p value < 0.05) changes over time in carbon cycle variables and driver data are shown for the growing season (GS, when SCA $< 50\,\%$ AND GEE < 0). Please note that as the growing season includes only the period of time for which vegetation is productive at any pixel (GEE < 0), periods of time for which air temperature extremes or drought hinder photosynthesis are not included. The influences of rising EVI and air temperatures on increasing Arctic rates of photosynthesis are therefore made clear, whereas plots of annual GEE (Fig. 7) emphasize reductions in photosynthetic uptake of C by forest vegetation.

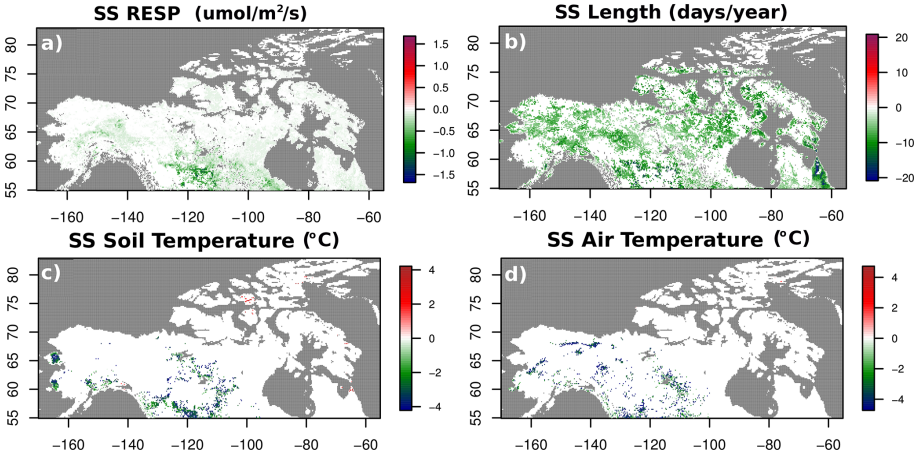

Figure 9. Sen's slope of median change (2001–2012) in PolarVPRM estimates of snow season (SS, when SCA $\geq 50\,\%$) carbon cycle variables, and driver data. Values are only shown for locations with a statistically significant change over time (p value < 0.05).